Supporting Information

Gupta et al. 10.1073/pnas.1309958110

SI Materials and Methods

Reagents. Pipes and Taxol (paclitaxel) were obtained from Sigma. GMPCPP was purchased from Jena Biosciences. Dolastatin-10 (DL; NSC# 376128) was a kind gift from the National Cancer Institute/Development Therapeutics Program Open Chemical Repository, National Cancer Institute (http://dtp.cancer.gov). All other chemicals were of analytical grade.

Cloning and Protein Purification. Human stathmin constructs were cloned into pET15b (Novagen) in a manner described previously (Fig. 1*A*) (1). The construct was verified by restriction-enzyme digestion and DNA sequencing analysis. Recombinant stathmin with a 6-histidine tag was expressed and purified from *Escherichia coli* BL21 (DE3) cells as described previously (1). The purity of the purified protein was assessed by SDS/PAGE (Fig. S1) and protein was quantified by comparison with standard amounts of BSA on Coomassie blue stained SDS/PAGE gels.

Preparation of Tubulin Polymers. Porcine brain tubulin was prepared by two cycles of polymerization and depolymerization as described previously (1). Phosphocellulose chromatography was used to remove the microtubule associated proteins from tubulin preparation.

Taxol (Tx) microtubule (MT) polymer was prepared from purified tubulin by the stepwise addition of Taxol, as described previously (1). Tx-MTs containing more protofilament structures [Tx-MT (MP)] were prepared as described previously (2) by incubating the tubulin (30 μM) plus 1 mM GTP in PEM buffer (80 mM Pipes, pH 6.8, 2.0 mM $MgCl_2$, and 1.0 mM EGTA) for 20 min at 37 °C. Then five volumes of PEM buffer containing 10 μM Taxol were added and samples were further incubated for 20 min at 37 °C. Tx-MT (fragmented) was prepared by shearing the Tx-MT polymers through a 30-gauge needle, as described previously (1). All taxol-treated polymer preparations were pelleted by ultracentrifugation at 100,000 × *g* for 15 min at 37 °C to remove unpolymerized tubulin and then resuspended in PEM buffer containing 10 μM taxol. All taxol-stabilized tubulin polymer experiments were performed in PEM buffer containing 10 μM Taxol.

GMPCPP MTs (CPP-MTs) were prepared by using the method described earlier (2, 3). Briefly, tubulin (15 μM) in PEM buffer with GMPCPP (0.5 mM) was incubated on ice for 10 min and then samples were centrifuged to remove any tubulin aggregates. GMPCPP-tubulin solutions were polymerized for 40 min at 37 °C. Polymers were sedimented at 100,000 × *g* for 15 min at 37 °C and then resuspended in PEM buffer. CPP-protofilaments (CPP-PFs) were prepared by depolymerization of CPP-MTs induced by the addition of one tenth volume of 0.4 M $CaCl_2$ (40-mM final concentration) to the CPP-MTs (12 μM) for 40 min at 37 °C (2, 3). Samples were centrifuged and resuspended in PEM buffer.

DL-rings were prepared as previously described with minor modifications (4). Tubulin (10 μM) was incubated with Dolastatin-10 (20 μM) in polymerization buffer [40 mM Pipes, pH 6.8, 1.5 mM $MgCl_2$, and 12% (vol/vol) dimethyl sulfoxide] for 1 h at 25 °C. Polymers were sedimented at 25 °C for 10 min at 100,000 × *g*. Pellet was resuspended in PEM buffer containing 5 μM Dolastatin-10. All DL-rings experiments were performed in the presence of 5 μM Dolastatin-10.

Zn-sheets were prepared as described earlier with some modification (5, 6). Briefly, tubulin (40 μM) was first polymerized in PEM buffer containing GTP (1.0 mM) and 4 M glycerol for 30 min at 37 °C. Polymers were pelleted at 100,000 × g for 15 min at 37 °C. The pellet was resuspended in cold Zn-Mes buffer (100 mM Mes, pH 6.0, 0.5 mM $MgCl_2$, 0.5 mM EGTA, 1.0 mM $ZnCl_2$, 0.1 mM DTT, and 3.0 mM GTP) and incubated on ice for 40 min to allow depolymerization. Formation of Zinc-sheets was induced by incubating the sample (2.0 mg/mL) at 30 °C for 20 min in the presence of 20 μM Taxol. Polymers were sedimented again at 25,000 × *g* for 10 min at 30 °C to remove the unpolymerized tubulin. Pellet was resuspended in Zn-Mes buffer containing 10 μM Taxol and used for further study. Zinc-sheets are found to be unstable at neutral pH perhaps because of the reduced solubility of $ZnCl_2$ (5), therefore, all Zn-sheets experiments were performed at pH 6.0 in Zn-Mes buffer containing 10 μM Taxol at 30 °C. For each set of experiments, tubulin polymers were prepared fresh from tubulin and never frozen.

Binding Measurements. The binding affinity of stathmin for the different tubulin polymers was measured by cosedimentation assays (1). Briefly, stathmin (2.0 μM) was incubated with varying concentrations of tubulin polymers (0–12 μM) in PEM buffer for 30 min at appropriate temperature and then centrifuged at 165,000 × *g* for 20 min. Equal fractions of both supernatants and pellets were separated on SDS/PAGE gels. Proteins were stained with Coomassie blue, digitally scanned, and the band intensity of stathmin was quantified with ImageJ (National Institutes of Health). The binding affinity was calculated as described previously (1). Briefly, binding data were fit to a bimolecular binding equation $Y = B_{max}X/(K_d + X)$, where Y is the fraction of stathmin in the pellet; X is the concentration of tubulin polymers, and B_{max} is the maximal achievable binding. All analyses were performed under the assumption of 2:1 stoichiometry (tubulin dimer:stathmin ratio as estimated from the 2:1 ratio observed in Fig. 2*B*), and B_{max} values were set to 1.0.

Computational Modeling. ***Description of the model.*** Simulations were performed using the detailed computational model of MT dynamics as previously described (7), using parameter set 3. Stathmin binding and detachment was simulated by introducing the existence of two new classes of tubulin subunits (GTP or GDP bound to stathmin) that converted reversibly with regular tubulin subunits (GTP or GDP as appropriate) and had binding and release kinetics consistent with the affinities as described in the main text; stathmin binding was allowed to occur only when pairs of longitudinally adjacent permissible binding sites were present. The stathmin-bound tubulin subunits interacted with the other subunits in the MT according the normal simulation rules, except for the changes to the particular rate constants as described in the main text. Except for the systems of MTs simulated in Fig. S5 and Table S2, all modeling results are derived from multiple simulations of single MTs performed under constant [free tubulin] and [free stathmin], as described.

Simulation of systems of dynamic microtubules. For Fig. S5 and Table S2, the model was modified to simulate a system of multiple MTs competing with each other for a limited pool of tubulin subunits, using approaches similar to those used in our previous work (8). The simulations were performed with or without a boundary representing a spatial constraint, such as a cell edge; interaction of MTs with this boundary induced catastrophe indirectly by preventing addition of further tubulin subunits and allowing GTP hydrolysis to catch up with the MT tip. As shown in our previous work (8), this premature induction of catastrophe by the boundary (cell edge) causes the concentration of free tubulin to rise above the natural steady-state concentration of free tubulin, inducing persistent MT growth if the system contains

a sufficiently large pool of active tubulin subunits (8). For each entry in Fig. S5 and Table S2, we simulated a system of 20 MTs in a reaction volume of 200 μm^3 containing 15 μM total tubulin, with (or without) a boundary at 16 μm, thus simulating a system that could be considered to mimic a wedge of a radial cell with $r = 16$ μm (computational constraints prevented simulation of a larger system).

Analysis of simulation results. Dynamic instability parameters were calculated as in ref. 7. Data in Fig. 4 and Table S1 represent means ± SD from three separate simulations of individual MTs, each run for more than 1 h of simulated time. Dynamic instability measurements in Table S2 represent averages ± SD for the 20 MTs in each simulation, with data acquisition commencing once polymer mass steady-state had been reached (~20 min of simulated time, as verified by plots of [polymer] as a function of time). Diffusion and drift in Table S2 were calculated as in ref. 9, using 1-min intervals; the averages and SDs reported in Table S2 each result from a set of five separate measurements taken 5 min apart after polymer length steady-state had been reached (~45 min for the cell-like systems, ~1.5 h for the in vitro-like systems). The length distributions in Fig. S5 were calculated in a similar manner.

Hardware. Simulations were performed on an Intel Core i3-2350M, 2.3 GHz with 6GB of memory, running Ubuntu 12.04. It took ~24 h of computer time to produce 2 h of simulated time for a system of 20 MTs.

Calculation of the fraction of 1 μM stathmin that is free to interact with PFs when 12 μM unpolymerized tubulin is present. One argument against the idea that stathmin can act by binding to PF structures at the MT tip is that under normal MT polymerization conditions, most of the stathmin will be occupied by tubulin subunits, and none will be free to bind to the PFs. To address this concern, we calculated the concentration of stathmin that would be free under these conditions, and then used the computational models to test whether this concentration of free stathmin would be predicted to have discernable effects.

To calculate the concentration of free stathmin, we used the following logic:

The standard first-order binding equation is [fraction stathmin bound] = [L]/([L] + K_d), where [L] is the concentration of free ligand (tubulin in this case) and K_d is the apparent affinity of the interaction between stathmin and tubulin dimers as reported in the literature. Here we will assume 0.5 μM, because the reported values range between 0.1 and 1μM (discussed in the main text).

Assuming 12 μM free tubulin, 1 μM stathmin, and $K_d = 0.5$ μM, the fraction of stathmin bound to tubulin is 96%, leaving 4% free. However, 96% occupancy of stathmin means that ~2μM of the tubulin is bound to stathmin, so the actual free concentration of tubulin is ~10 μM.

Assuming 10 μM free tubulin, 1 μM stathmin, and $K_d = 0.5$ μM, the fraction of stathmin bound to tubulin is 95%, leaving 5% free to interact with PFs.

Thus, we used 0.05 μM free stathmin for the simulations of Fig. 4*D*, Fig. S5, and Table S2, all of which were assumed to occur in the presence of 12 μM unpolymerized tubulin and 1 μM total stathmin.

SI Results and Discussion

Before interpreting the effects of stathmin activities in the simulated systems of dynamic MTs, it is important to consider two aspects of dynamic MT systems: First, previous work has shown that although MTs in vitro exhibit normal dynamic instability and have an exponentially decaying length distribution (where short MTs are more frequent than long MTs), MTs in interphase cells grow persistently and exhibit an inverted length distribution (where long MTs are more frequent than short ones) (9; see also ref. 8). One possible explanation of these phenomena is that MT binding proteins cause the persistent growth in vivo. However, our work with a simplified model of MT dynamics acting in a cell-like (spatially constrained) system provided evidence that the persistent MT growth and inverted length distribution characteristic of the in vivo systems could be caused simply by putting enough tubulin in a confined space (8). The explanation for this observation is that the cell edge induces catastrophe earlier than it would otherwise occur, causing the steady-state concentration of free tubulin to rise above the natural steady-state concentration (the critical concentration); this increase in [free tubulin] induces persistent growth by suppressing catastrophe and enhancing rescue (8).

Second, the logic above suggests that stathmin's sequestration activity could have a major impact on MT behavior in vivo because the relatively small perturbation in [total active tubulin] caused by 1 μM stathmin could potentially be sufficient to shift a MT system from the persistent growth characteristic of interphase MTs to the short and dynamic MTs characteristic of mitosis (the computational models predict that the transition between persistent growth and nonpersistent growth occurs over a relatively small range of [free tubulin]; see figure 4*B* of ref. 8). In contrast, the sequestration activity would be expected to have little effect on MT dynamics in a system of MTs lacking spatial constraint (i.e., in vitro) because classic understanding of polymer critical concentration states that the concentration of free tubulin at steady-state does not depend on the amount of input tubulin once the critical concentration of subunits has been placed in the system. This logic implies that MT dynamics in vitro should be the same with or without stathmin's sequestering activity because addition of sequestering stathmin should simply result in less polymer. In either case (with or without spatial constraint), the direct activity might be expected to add to the effect of the sequestering activity, but it was not clear what the relative magnitude of the effect would be.

These considerations suggested that it would be worthwhile to test the relative effectiveness of the sequestration and direct activities of stathmin as discussed in the main text, and to do so in environments with and without spatial constraints. These data are presented in Figure S5. To prepare this figure, we modified the computer model used in Fig. 4 so that it could simulate a set of many MTs competing for a limited pool of tubulin subunits, with and without a barrier (cell edge). More specifically, the system consisted of 20 MTs in a volume of 200 μM^3 with 15 μM total tubulin and 1 μM total stathmin, with or without a barrier at 16 μm. This system could be considered to mimic a wedge of a radial cell with radius 16 μm (computer constraints prohibited simulating a larger systems). Other aspects of the simulation were similar to the simulation in Fig. 4*D*, including the assumption that 1 μM total stathmin corresponds to 0.05 μM free stathmin (see simulation discussion in *SI Materials and Methods* for details).

1. Gupta KK, et al. (2009) Minimal plus-end tracking unit of the cytoplasmic linker protein CLIP-170. *J Biol Chem* 284(11):6735–6742.
2. Elie-Caille C, et al. (2007) Straight GDP-tubulin protofilaments form in the presence of taxol. *Curr Biol* 17(20):1765–1770.
3. Müller-Reichert T, Chrétien D, Severin F, Hyman AA (1998) Structural changes at microtubule ends accompanying GTP hydrolysis: Information from a slowly hydrolyzable analogue of GTP, guanylyl (alpha,beta)methylenediphosphonate. *Proc Natl Acad Sci USA* 95(7):3661–3666.
4. Moores CA, Milligan RA (2008) Visualisation of a kinesin-13 motor on microtubule end mimics. *J Mol Biol* 377(3):647–654.
5. Kamimura S, Mandelkow E (1992) Tubulin protofilaments and kinesin-dependent motility. *J Cell Biol* 118(4):865–875.

6. Kawachi A, et al. (2003) Different protofilament-dependence of the microtubule binding between MAP2 and MAP4. *Biochem Biophys Res Commun* 305(1):72–78.
7. Margolin G, et al. (2012) The mechanisms of microtubule catastrophe and rescue: Implications from analysis of a dimer-scale computational model. *Mol Biol Cell* 23(4): 642–656.
8. Gregoretti IV, Margolin G, Alber MS, Goodson HV (2006) Insights into cytoskeletal behavior from computational modeling of dynamic microtubules in a cell-like environment. *J Cell Sci* 119(Pt 22):4781–4788.
9. Komarova YA, Vorobjev IA, Borisy GG (2002) Life cycle of MTs: Persistent growth in the cell interior, asymmetric transition frequencies and effects of the cell boundary. *J Cell Sci* 115(Pt 17):3527–3539.
10. Cassimeris L (2002) The oncoprotein 18/stathmin family of microtubule destabilizers. *Curr Opin Cell Biol* 14(1):18–24.
11. Amayed P, Pantaloni D, Carlier MF (2002) The effect of stathmin phosphorylation on microtubule assembly depends on tubulin critical concentration. *J Biol Chem* 277(25): 22718–22724.

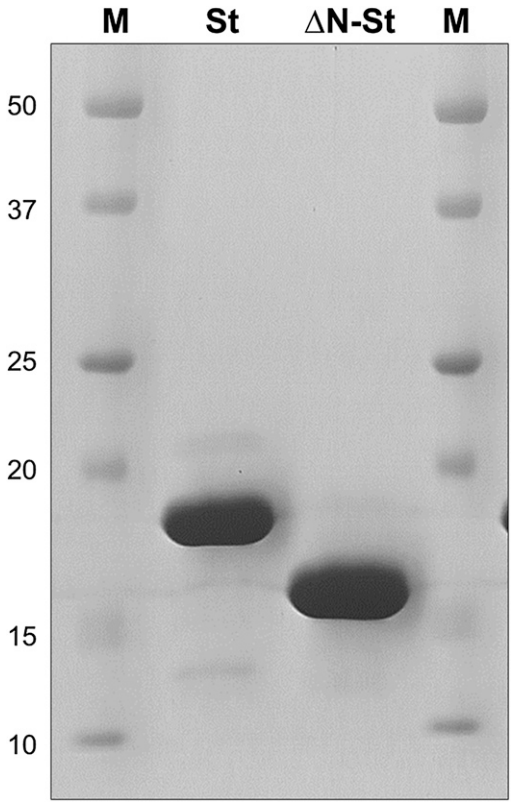

Fig. S1. SDS/PAGE of purified His-tagged stathmin proteins (~10 μg) used in this work. Molecular weight markers (M) are shown in kilodaltons.

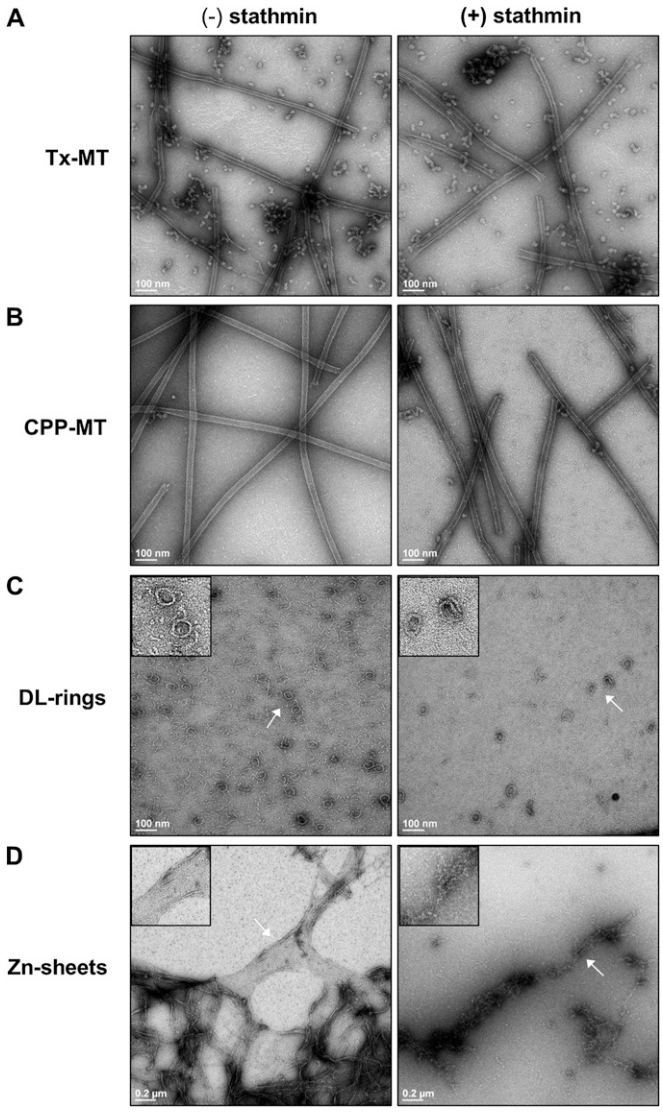

Fig. S2. Electron micrographs of various tubulin polymers as indicated (see main text for more discussion of these polymer types). (*A* and *B*) Tx-MTs and CPP-MTs did not appear to be altered by stathmin (compare *Left* and *Right*). (*C*) In the absence of stathmin (*Left*) DL-rings appeared as described in many other reports (e.g., ref. 4). In the presence of stathmin (*Right*), individual rings were visible and they appeared similar to the DL-rings without stathmin (compare *Right* and *Left*). (*Insets*) Magnifications (2.5×) of the structures indicated by the arrows. (*D*) In the absence of stathmin (*Left*), Zn-sheets appeared as a mixture of flat sheets and what seem to be folded sheet-like structures, similar to previous reports (5). In the presence of stathmin (*Right*), it was difficult to find any structures at all, but those structures that did appear were very different from those found in the absence of stathmin (compare *Right* and *Left*). (*Insets*) Magnifications of the structures indicated by the arrows. Note: After considerable effort, we found that we were not able to get interpretable images of CPP-PF, with or without stathmin, perhaps because visualization of these structures requires unusual fixations and imaging techniques (2). Tubulin polymers were prepared in the absence and presence of stathmin (8.0 μM) as described in Fig. 2*A*. After 30-min incubation, all samples were negatively stained for EM analysis as described previously (1). All images were acquired at 27,000× magnification (Scale bar, 0.1 μm) except Zn-sheets that were taken at 13,000× magnification (Scale bar, 0.2 μm). The images shown are representative of the structures observed, except as noted above.

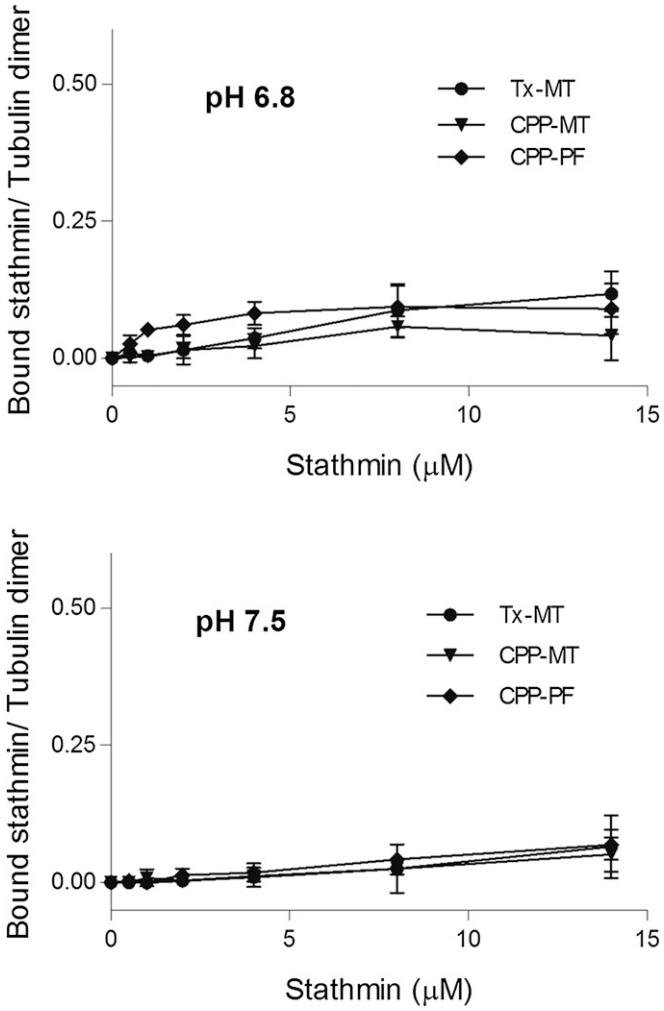

Fig. S3. Analysis of the tubulin:stathmin stoichiometry for stathmin sedimenting with different tubulin polymers. The binding stoichiometry of stathmin to tubulin dimer in various polymers (except DL-rings, which was presented in Fig. 2*D*) were determined as described in Fig. 2*D*. Data are the average of three independent experiments. Values are presented ± SD. These data show that stathmin bound weakly to the indicated tubulin polymers at either pH.

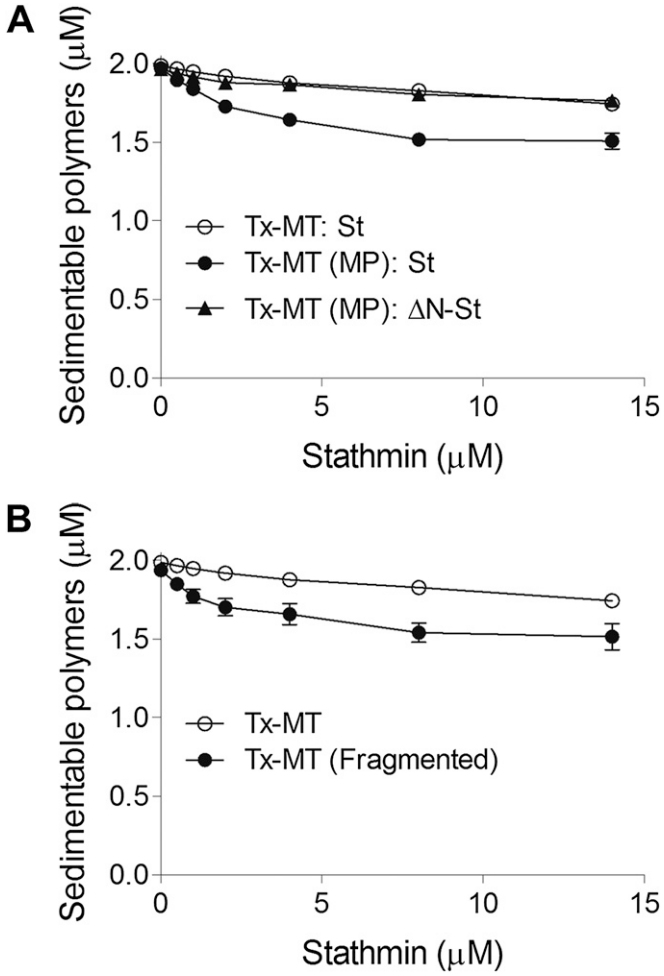

Fig. S4. Effects of stathmin on depolymerization of taxol stabilized tubulin polymers. Various concentrations of stathmin or Δ*N*-stathmin (0–14 μM) as indicated were incubated with either Tx-MT (MP) (*A*) or Tx-MT (fragmented) (*B*) in PEM buffer containing 10 μM Taxol. Samples were sedimented and the amount of depolymerized tubulin was calculated as described in Fig. 2. Data are the average of three independent experiments and presented as mean ± SD. The Tx-MT data from Fig. 2*B* are included for comparison. These data show that both Tx-MT (MP) and Tx-MT (fragmented) polymers are more sensitive to stathmin than regular Tx-MT.

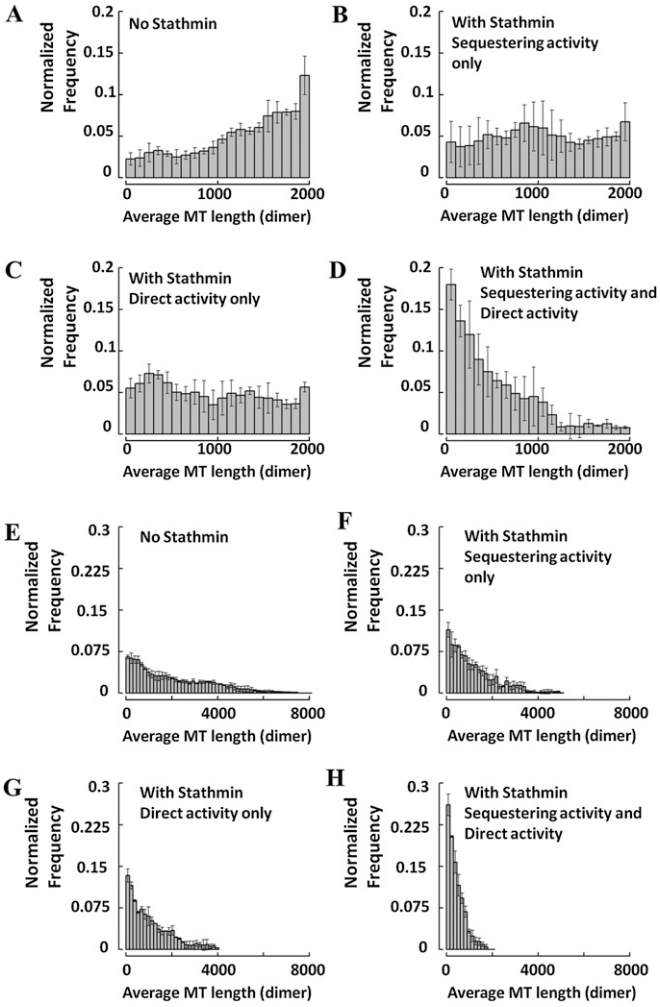

Fig. S5. Effect of stathmin's sequestering and direct activities on microtubules in a cell-like (spatially-constrained) system. Each of the panels in the figure shows the distribution of MT lengths in a simulation run with a different stathmin activity (as indicated) and otherwise identical conditions: (*A–D*) Simulations performed in the cell like environment (i.e., with the barrier at 16 μm) with stathmin activities as indicated; (*E–H*) A parallel set of control simulations performed without a barrier. *A* shows that in the cell-like system without any stathmin activity, there were more long MTs than short MTs, as is expected for an MT system growing persistently, and persistent growth was indeed demonstrated by a positive drift coefficient (1.4 ± 0.4 μM/min) (see Table S2; the measurement and interpretation of drift coefficients is discussed by ref. 9). *B* and *C* show that addition of either a 1-μM sequestering activity (simulated by dropping the total tubulin concentration to 13 μM) or a 0.05-μM direct activity changed the length distributions to ones that were more nearly flat; consistent with this change, these systems exhibited small positive drift coefficients (Table S2). The observation that these stathmin activities could each significantly alter the morphology and behavior of the simulated MT systems provides evidence that both the sequestering and direct activities are likely to be relevant in a cellular context. *D* shows that combination of the sequestering and direct stathmin activities shifted the MT length distribution significantly, to one that had a preponderance of short MTs and had the shape of an exponential decay. As expected from this distribution, the drift coefficient for this system was zero (Table S2). This observation provides evidence that the sequestering and direct activities can work in an additive way. *E–H* show that in the parallel simulated system without a barrier, the stathmin activities do shift the length distribution toward shorter MTs, and do so in an additive way. However, they have no effect on the drift coefficient: in all cases, the drift coefficient is zero (Table S2), as expected or an unconstrained system at steady-state. Taken together, these observations provide evidence that the sequestering and direct activities work together to generate stathmin's observed effects in vivo and in vitro. The in vivo concentration of stathmin has been reported to range more than 100×, between 0.005% and 0.5% of cell protein (reviewed by ref. 10). At least one other study that aimed to use in vivo concentrations of stathmin in vitro chose 6 μM (11). Therefore, we chose 1 μM for our studies here as a high but still relatively conservative estimate.

Table S1. Effect of stathmin molecules with various activities on the behavior of MTs in the computer simulations

	Observed dynamic instability parameter							
Stathmin activity	V_{grow} (dimers per second)	V_{grow} SD	V_{short} (dimers per second)	V_{short} SD	F_{cat} (events per second of growth)	F_{cat} SD	F_{res} (events per second of depolymerization)	F_{res} SD
Effect on MTs when stathmin binds to longitudinal pairs of dimers in regions of PF that have no lateral bond								
No stathmin	5.56	0.060	69.59	1.40	0.008	0.001	0.010	0.005
K_d = 1 μM, no effect	5.59	0.074	69.34	1.34	0.010	0.001	0.010	0.004
K_d = 1 μM, k_{bond} ↓ 2×	4.95	0.231	71.38	2.32	0.024	0.002	0.003	0.001
K_d = 1 μM, k_{bond} ↓ 2×, kh ↑ 10x	4.77	0.464	70.09	4.15	0.029	0.005	0.000	0.000
K_d = 1μM, kbond ↓ 2×, kshort ↑ 10x	5.09	0.142	69.85	3.80	0.025	0.001	0.000	0.000
No stathmin	5.56	0.060	69.59	1.40	0.008	0.001	0.010	0.005
K_d = 1 μM, kg ↓ 2×	5.33	0.150	69.87	1.62	0.014	0.001	0.009	0.004
K_d = 1 μM, k_{bond} ↓ 2×, kg ↓ 2×	4.83	0.061	71.78	4.39	0.025	0.002	0.003	0.001
K_d = 1 μM, k_{bond} ↓ 2×, kg ↓ 5×	3.82	0.262	71.48	6.96	0.028	0.003	0.003	0.001
K_d = 0.5 μM, k_{bond} ↓ 2×	3.92	0.065	72.08	1.96	0.030	0.001	0.000	0.000
K_d = 0.5 μM, kg ↓ 2×	5.12	0.323	69.80	1.68	0.018	0.003	0.010	0.004
K_d = 0.5 μM, k_{bond} ↓ 2×, kg ↓ 2×	3.76	0.362	73.05	4.30	0.033	0.001	0.000	0.000
K_d = 0.5 μM, k_{bond} ↓ 2×, kg ↓ 5×	MTs too short to be measured							
Stathmin binds to longitudinal pairs of dimers anywhere on the MT								
No stathmin	5.56	0.060	69.59	1.40	0.008	0.001	0.010	0.005
K_d = 25 μM, no effect	5.56	0.006	69.12	1.88	0.010	0.001	0.009	0.004
K_d = 25 μM, k_{bond} ↓ 2×	5.61	0.140	68.85	1.01	0.010	0.004	0.011	0.007
K_d = 25 μM, k_{bond} ↓ 2×, kh ↑ 10x	5.38	0.104	69.84	0.48	0.010	0.001	0.010	0.005
K_d = 25 μM, k_{bond} ↓ 2×, ks ↑ 10x	5.55	0.057	69.83	2.25	0.010	0.002	0.010	0.003
K_d = 25 μM, k_{break} ↑ 10×	5.50	0.031	70.59	2.76	0.011	0.003	0.010	0.005

Stathmin binds to longitudinal pairs of dimers in regions of PF that have no lateral bonds . k_{bond} and k_{break} control the rate of lateral bond formation and breakage respectively, whereas k_s and k_g control longitudinal bond formation and breakage. Data are from average values (± SD) taken from length-history plots derived from three independent runs in which the plus end of a single MT (nucleated from a stable seed) was simulated for more than 1 h of elapsed time. The simulations occurred under conditions of constant [free tubulin] and [free stathmin] and were performed using parameter set 3 of Margolin et al. (7) with the modifications to test stathmin activity, as described above.

Table S2. Dynamic instability parameters and other data extracted from the simulations shown in Fig. S5

Behavior of microtubules	No stathmin	Stathmin sequestration activity only	Stathmin direct activity only	Both sequestration and direct activities
Behavior of microtubules in a cell-like (spatially constrained) system with stathmin activities as indicated				
V_g (μm/min)	3.85 ± 0.02	3.2 ± 0.1	2.93 ± 0.04	2.45 ± 0.05
V_s (μm/min)	33.8 ± 0.3	33.5 ± 0.5	34.3 ± 0.7	34.5 ± 0.5
Drift (μm/min)	1.2 ± 0.4	0.07 ± 0.1	0.03 ± 0.1	0.00 ± 0.3
Diffusion (μm^2/min)	3.4 ± 0.3	2.7 ± 0.8	2.0 ± 0.5	1.9 ± 0.6
F_{cat} (events per second of growth)	0.0010 ± 0.0003	0.003 ± 0.001	0.006 ± 0.002	0.011 ± 0.002
F_{res}(events per second depolymerization)	0.06 ± 0.01	0.03 ± 0.01	0.05 ± 0.01	0.03 ± 0.01
[Free tubulin] (μM)	12.1 ± 0.1	10.8 ± 0.2	13.0 ± 0.08	12.1 ± 0.2
[Tubulin polymer] (μM)	2.9 ± 0.1	2.2 ± 0.2	2.0 ± 0.08	0.9 ± 0.2
Sequestered tubulin	0	2 μM (defined)	0	2μM (defined)
Behavior of microtubules in an in vitro-like system (no spatial constraint) with stathmin activities as indicated				
V_g (μm/min)	3.23 ± 0.03	3.03 ± 0.02	2.77 ± 0.03	2.52 ± 0.03
V_s (μm/min)	33.6 ± 0.6	33 ± 0.5	33.8 ± 0.7	33.7 ± 0.3
Drift (μm/min)	0.0 ± 0.1	0.0 ± 0.1	0.0 ± 0.1	0.0 ± 0.1
Diffusion (μm^2/min)	3.5 ± 0.2	2.5 ± 0.5	2.36 ± 0.4	2.0 ± 0.6
F_{cat} (events per second of growth)	0.004 ± 0.001	0.006 ± 0.002	0.008 ± 0.002	0.012 ± 0.002
F_{res}(events per second depolymerization)	0.03 ± 0.01	0.02 ± 001	0.04 ± 0.01	0.03 ± 0.01
[Free tubulin] (μM)	10.6 ± 0.1	10.5 ± 0.1	12.4 ± 0.2	11.9 ± 0.1
[Tubulin polymer] (μM)	4.4 ± 0.1	2.5 ± 0.2	2.6 ± 0.2	1.1 ± 0.1
[Sequestered tubulin]	0	2 μM (defined)	0	2 μM (defined)

Simulations in both sections of the table were performed under identical conditions (15 μM total tubulin, 1 μM stathmin with activities as indicated, 20 MTs nucleated from stable GMPCPP-like seeds), except that those in the upper section were run in a "cell" with a radius of 16 μm, whereas those in the lower section were run without spatial constraint. As in Fig. S5, sequestration of 2 μM tubulin by 1 μM stathmin was simulated by reducing the concentration of total active tubulin to 13 μM in simulations as indicated. Note that in both sections, MTs compete for a limited pool of total tubulin, making these simulations differ from those in Table S1, where [free tubulin] was held constant. The resulting variation in [free tubulin] increases the SD within a given simulation, and complicates interpretation of stathmin-induced changes to DI parameters. Data are average values (± SD) extracted from length-history plots of the 20 MTs in each system as simulated for more than 1 h of elapsed time (all systems had achieved polymer mass steady-state before measurements were taken). The legend to Fig. S5 has additional information. These data, together with Fig. S5, provide evidence that both the sequestering and direct activities are likely to be relevant in a cellular context and that the activities work together to create stathmin's overall activity.